Metal Removal from Synthetic Mine Tailing Leachates using Fixed-Bed Ion-Exchange Columns

Alex L. Riley*, Sarah E. Pepper, Ella L. Sexton and Mark D. Ogden

Separations and Nuclear Chemical Engineering Research (SNUCER) Group,
Department of Chemical and Biological Engineering, University of Sheffield, United Kingdom

**Corresponding author: ariley4@sheffield.ac.uk*

The generation and disposal of solid wastes from the mining industry has the potential to cause significant, enduring environmental damage. Atmospheric weathering of waste stockpiles leads to the formation of metal-rich leachates, which have been shown to adversely affect ecological communities, and can act as barriers towards meeting legislative water quality targets. The removal of problematic metals from tailings prior to disposal may pose an opportunity to prevent this damage. This research presents results from dynamic column experiments aimed at assessing the performance of several commercial ion-exchange resins for metal removal from simulated tailing leachates. Artificial mixed-metal solutions were prepared to simulate the conditions expected following a sulphuric acid leach of mine tailings. Metal breakthrough from each column was modelled to gain an insight to the selectivity and capacity of each tested resin, allowing identification of the most-suitable resins to take forward to process optimisation and scale-up.

INTRODUCTION

The process of mining, while essential for global mineral resource supply chains, is inherently associated with the potential risk for environmental damage; particularly towards surface waters and aquifers. In the United Kingdom, it has been conservatively estimated that 6% of surface water bodies nationally are adversely affected by mine waters (Mayes *et al.*, 2009), predominantly from abandoned mine workings. Following mine abandonment, the management options available are dependent on several factors, such as the morphology of the mine network and the local hydrogeology (Westermann *et al.*, 2017). Given that most metal mines in the United Kingdom were abandoned following their peak production in the 18th and 19th centuries (Crane *et al.*, 2016), pumping capabilities are rarely available, and groundwater resurgence leads to uncontrolled discharge of metalliferous waters in many cases (Banks *et al.*, 2017). The effects of such releases include the damage of downstream ecological communities, adverse effects on chemical water quality, and potential degradation of public supply aquifers where groundwaters are contaminated (Armitage *et al.*, 2007; Byrne *et al.*, 2013; Neymeyer *et al.*, 2007).

The generation of metal-rich waters, both during active mine working and following abandonment, is related to the interaction of previously unexposed mineral surfaces with resurging groundwater, as described below for pyrite, FeS_2 (Kruse *et al.*, 2013; Younger *et al.*, 2002). The pyritic oxidation process occurs in four stages: oxidation and dissolution of exposed pyrite (Equation 1); conversion of ferrous iron to ferric iron (Equation 2); hydrolysis of ferric iron (Equation 3); and further pyritic oxidation by

aqueous ferric iron (Equation 4). Mineral oxidation reactions may also be accelerated in the presence of certain lithotrophic bacteria (Johnson and Hallberg, 2003).

$$2\,FeS_{2\,(s)} + 7\,O_{2\,(aq)} + 2\,H_2O_{(l)} \rightarrow 2\,Fe^{2+}_{(aq)} + 4\,SO^{2-}_{4\,(aq)} + 4\,H^{+}_{(aq)} \quad [1]$$

$$2\,Fe^{2+}_{(aq)} + 0.5\,O_{2\,(aq)} + 2\,H^{+}_{(aq)} \rightarrow Fe^{3+}_{(aq)} + H_2O_{(l)} \quad [2]$$

$$2\,Fe^{3+} + 6\,H_2O_{(l)} \rightarrow 2\,Fe(OH)_{3\,(s)} + 6\,H^{+}_{(aq)} \quad [3]$$

$$14\,Fe^{3+} + FeS_{2\,(s)} + 8\,H_2O_{(l)} \rightarrow 2\,SO^{2-}_{4\,(aq)} + 15\,Fe^{2+}_{(aq)} + 16\,H^{+}_{(aq)} \quad [4]$$

It is the products of the above reactions that give mine waters their physicochemical characteristics; namely, a low pH, high sulphate concentration, and propensity for rapid precipitation of secondary minerals (e.g., iron hydroxides (Equation 3)). The acid conditions within underground mine systems promote the dissolution of other metal-bearing mineral deposits in the host rock (Wolkersdorfer, 2008), leading to elevated concentrations of metals such as copper, manganese, nickel, and zinc in mine waters. Additionally, where the pH of waters is below pH 4, the reaction of clay minerals can result in increased aluminium concentrations within effluent waters (Banks *et al.*, 1997). Given the variation of geology within mines from different geographical areas, the elemental composition of mine waters also varies from region to region (Mayes *et al.*, 2010).

In addition to the flooding of disused mine systems, mine tailings can act as a source of metalliferous leachates. Mine tailings are the solid waste byproducts of mining and are commonly disposed of in custom-built tailing facilities. In instances where tailings are heaped and open to the atmosphere, the percolation of rainwater through the heap can instigate weathering reactions similar to those previously described, resulting in leachate formation. Given the adverse effects of mine waste leachates on the environment, the removal of contaminant metals is a priority; both from waters being discharged from mine adits and from tailing heap leachates. Furthermore, should the metal contaminants be leached and recovered from the solid mine tailings themselves in a controlled manner prior to dumping, the risk of environmental damage from mine wastes could be reduced.

The research presented here aims to investigate the suitability of a range of commercially available ion-exchange resins to remove the problematic metals encountered in mine tailing leachates. Building upon previous work by the authors, this paper presents the results of dynamic column experiments from mixed-metal solutions, with the eventual aim of creating a multi-column ion-exchange system for the treatment of aqueous mine wastes.

EXPERIMENTAL

Resin and Solution Preparation

The ion-exchange resins were either kindly donated by Purolite Ltd. (S930, S950, S957) or purchased from Sigma-Aldrich (M4195). Key specifications of each resin used are provided in Table I, as given by manufacturer specification sheets. Before column packing, resins were preconditioned to their hydrogen form by batch contact with excess 1 M sulphuric acid for 24 h on an orbital shaker. Preconditioned resins were washed multiple times with deionised water to ensure complete removal of residual sulphuric acid.

A solution was prepared by dissolving sulphate salts of Al^{3+}, Co^{2+}, Cu^{2+}, Fe^{3+}, Mn^{2+}, Ni^{2+} and Zn^{3+}, chosen to represent the metals more commonly associated with mine wastes. The solution was acidified to pH 1.43 (identified in previous experiments to be appropriate for efficient metal removal by the studied resins) using dilute sulphuric acid. Concentrations used for experiments were artificially high (200 mg/L per metal) to reduce experimental run time, and all metal concentrations were equal to limit any effects related to concentration difference between metal species.

Table I: Key characteristics of ion-exchange resins used (N/A = data not available from supplier, PS-DVB = polystyrene-divinylbenzene); capacities converted to eq/L from manufacturer specification sheets.

Resin	Acronym	Functionality	Capacity (eq/L)	Polymer matrix	Moisture (%)	Particle size (μm)
Dowex M4195	M4195	Bis-picolylamine	1.1-1.3	PS-DVB	40-60	297-841
Puromet MTS9300	S930	Iminodiacetic acid	1.6	PS-DVB	52-60	425-1000
Puromet MTS9500	S950	Aminophosphonic acid	1.3	PS-DVB	60-68	*N/A*
Puromet MTS9570	S957	Phosphonic/sulphonic acid	0.64	PS-DVB	55-70	*N/A*

Column Setup

Small-scale columns (Sorbtech flash cartridge, 5 mL) were packed with each ion-exchange resin and capped at either end with Teflon frits, resulting in a bed volume of 5 mL wet-settled resin per column. During packing, intermittent agitation of the resin promoted a homogenous distribution of particle size throughout the bed. A reverse-flow setup was employed to ensure efficient mass transfer between the solution and resin, whereby the solutions were introduced at the bottom of the column and pumped upwards against gravity. A Heidolph 'Hei-Flow Value 01' peristaltic pump with 'SP Quick' pump head was used to pass solutions through the column at a constant rate (10 BV/h), with effluents collected using a BioRad Model 2110 fraction collector. Initial solutions and treated samples were diluted using a 1% nitric acid solution prior to metals analysis by inductively coupled plasma optical emission spectroscopy (ICP–OES).

Breakthrough Modelling

Three commonly applied breakthrough models were used to analyse the breakthrough curves generated by each column experiment; the Modified Dose Response model (Equations 5 and 6), the Bohart–Adams model (Equation 7) and the Thomas model (Equation 8) (Albadarin *et al.*, 2012; Hamdaoui, 2009). Symbol definitions are provided in the *Nomenclature* section.

$$\frac{C_t}{C_o} = 1 - \left(\frac{1}{1+\left(\frac{F_t}{b}\right)^a}\right) \quad [5]$$

$$Q_o = \frac{bC_o}{m} \quad [6]$$

$$\frac{C_t}{C_o} = \left(\frac{e^{(K_a C_o t)}}{e^{(K_a C_o t)} + e^{(K_a (W/F))} - 1}\right) \quad [7]$$

$$\frac{C_t}{C_o} = \frac{1}{1+e^{\left(\frac{K_t Q_o m}{F} - K_t C_o t\right)}} \quad [8]$$

RESULTS

Weak Base Resin – M4195

The low retention of Al^{3+}, Mn^{2+} and Fe^{3+} ions within the M4195-packed column resulted in complete breakthrough ($C_t/C_o > 1$) after contact with 30 mL of solution, equating to six bed volumes (Figure 1). Suppressed breakthrough of Zn^{2+} and Co^{2+} indicated a stronger affinity of these metals towards the bis-picolylamine functional groups of M4195. The concentration ratio of most metals exceeded unity shortly after reaching complete breakthrough; an indication that metals had switched from being loaded to being displaced from the resin. The displacement of metals is indicative of the selectivity of each resin, with ions of lower affinity being displaced by those with higher affinity towards the functional group – a principal often encountered in instances where multiple metal species compete for sorbent sites (Escudero *et al.*, 2013). A high selectivity towards Ni^{2+} ions by M4195 was observed

(Figure 1) and, given that Cu^{2+} concentration in effluent solutions remained below limits of detection, it can be assumed that this resin has the highest selectivity towards copper over the other metals.

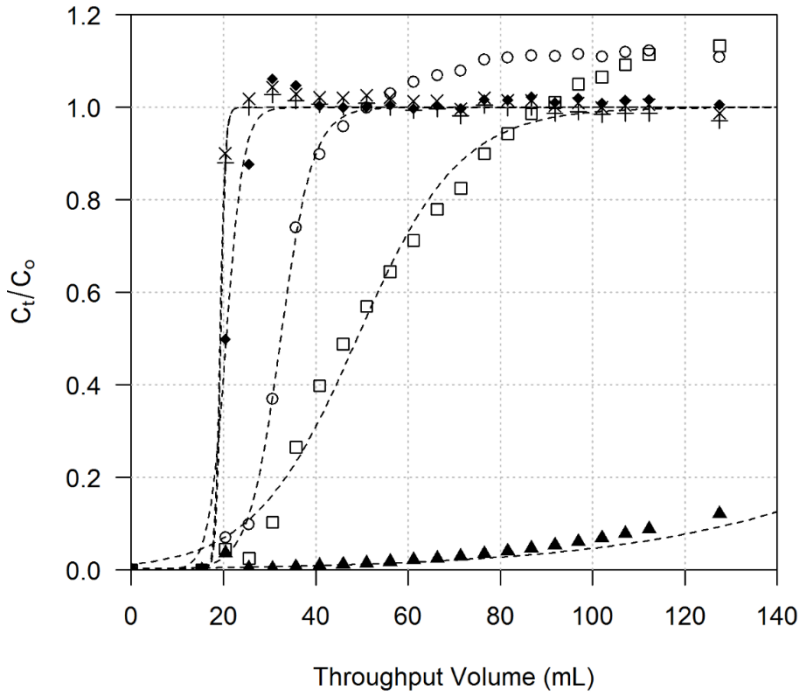

Figure 1: Breakthrough curves of metals after passing through M4195 column at pH 1.43. (Al^{3+} = +, Co^{2+}= □, Fe^{3+} = ♦, Mn^{2+} = ×, Ni^{2+} = ▲, Zn^{2+}= ○. Note: Cu^{2+} concentrations remained below limits of detection. Dotted lines represent model fitting (marked by an asterisk in Table II).

Modelling of breakthrough curves confirmed that lower operating capacities (Q_o) were associated with metals that showed faster breakthrough (Table II). It is important to note that the common breakthrough models are designed for single-species solutions, where C_t/C_o cannot exceed 1. It is for this reason that the modelled breakthrough curves in the presented figures are not able to exceed this value. Despite this, the breakthrough models used here showed reasonably good fits for most metals (Table II). Low R^2 values for Cu^{2+} modelling are symptomatic of the limited variation in data points, where maximum concentration ratio reached only 0.02 (data not presented in Figure 1).

Table II: Selected model parameters from breakthrough analysis of M4195. Asterisk (*) indicates that the model fit is displayed in Figure 1.

	Modified dose response				Bohart–Adams			Thomas		
	a	*b*	Q_o	R^2	K_a	*W*	R^2	K_t	Q_o	R^2
Al^{3+}	35.78	19.3	1.84	*0.997*	0.45	4.42	*0.997**	0.4	1.84	*0.997*
Co^{2+}	4.63	47.04	3.99	*0.971*	0.02	9.97	*0.985**	0.02	4.59	*0.982*
Fe^{3+}	11.29	20.51	1.64	*0.989*	0.14	3.94	*0.992**	0.14	1.64	*0.992*
Mn^{2+}	45.39	19.43	1.54	*0.993*	0.51	3.64	*0.996**	0.51	1.52	*0.996*
Ni^{2+}	5.76	208.24	16.96	*0.964*	0.01	41.42	*0.978**	0.01	17.28	*0.978*
Zn^{2+}	9.66	32.19	2.63	*0.955*	0.08	6.34	*0.964**	0.08	2.65	*0.964*

Weak Acid Resins – S930, S950

During loading of the S930-packed column, the only metal to reach complete breakthrough was Zn^{2+}, which exceeded C_t/C_o after 32 mL (6.4 BV) of solution had been pumped through (Figure 2).

Adsorption of other metals in solution (Al^{3+}, Co^{2+}, Fe^{3+}, Mn^{2+} and Ni^{2+}) exhibited the typical breakthrough curve shape, but concentration ratios remained below 1. This suggests multiple species were bound to the resin throughout the experiment, although there was a slight upward trend in concentration ratio, which is likely a result of the steadily increasing Cu^{2+} loading (Figure 2). It is expected that the metals with lower affinity for the iminodiacetic acid functionality, e.g., Zn^{2+}, Co^{2+}, Al^{3+}, Mn^{2+} (Riley *et al.,* 2018) would be displaced first as Cu^{2+} consumes resin capacity. The extraction of Fe^{3+} by S930 at low pH has been reported previously (e.g., Amphlett *et al*., 2018, Riley *et al*., 2018), lending explanation to the slightly suppressed breakthrough when compared to other metals studied (with exception of Cu^{2+}).

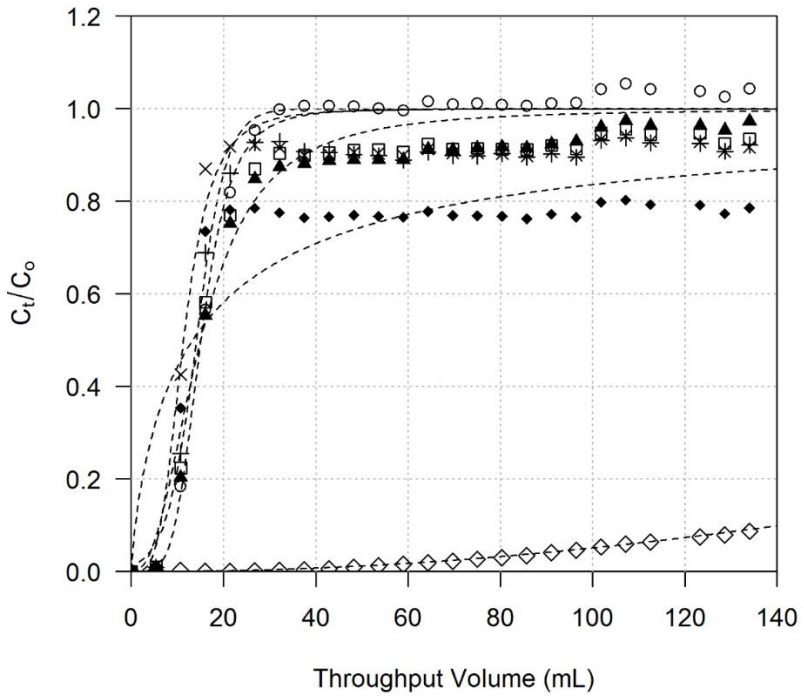

Figure 2: Breakthrough curves of metals after passing through S930 column at pH 1.43. (Al^{3+} = +, Co^{2+}= □, Cu^{2+} = ◊, Fe^{3+} = ♦, Mn^{2+} = ×, Ni^{2+} = ▲, Zn^{2+}= ○. Dotted lines represent model fitting (marked by an asterisk in Table III).

Breakthrough modelling indicated that S930 had a notably higher operating capacity towards Cu^{2+} over the other metals (Table III). The low R^2 values indicate that the available models were not able to satisfactorily describe metal adsorption for Fe^{3+}, Mn^{3+} and Al^{3+}; a result of the presence of competing ions.

Table III: Selected model parameters from breakthrough analysis of S930. Asterisk (*) indicates that the model fit is displayed in Figure 2.

	Modified dose response				Bohart–Adams			Thomas		
	a	*b*	Q_o	R^2	K_a	*W*	R^2	K_t	Q_o	R^2
Al^{3+}	1.9	12.45	1.31	*0.884*	0.07	3.18	*0.855*	0.08	1.48	*0.855**
Co^{2+}	2.42	15.02	1.43	*0.938**	0.06	3.26	*0.897*	0.06	1.51	*0.897*
Cu^{2+}	2.11	397.82	34.89	*0.997**	0.004	55.31	*0.969*	0.005	25.8	*0.969*
Fe^{3+}	0.81	13.28	1.15	*0.630**	0.004	8.43	*0.289*	0.005	0	*0.284*
Mn^{2+}	3.74	11.32	1.00	*0.841**	0.12	2.18	*0.828*	0.13	1.02	*0.828*
Ni^{2+}	2.26	15.64	1.44	*0.951**	0.05	3.29	*0.897*	0.06	1.52	*0.897*
Zn^{2+}	4.65	15.09	1.40	*0.992**	0.08	3.1	*0.991*	0.08	1.45	*0.991*

Metal adsorption to the aminophosphonic acid functional groups of S950 appeared to favour the trivalent transition metals. The order that metals reached complete breakthrough ($C_t/C_o = 1$) from the column was $Ni^{2+} > Co^{2+} > Zn^{2+} > Mn^{2+} > Cu^{2+}$, while Al^{3+} and Fe^{3+} did not exceed a C_t/C_o value greater than 0.8. Beyond 100 mL (20 BV) solution throughput, all divalent metal species had begun to be displaced from the column (Figure 3) by Al^{3+} and Fe^{3+} ions. This order of selectivity matches closely the extraction profiles observed under static conditions (Riley *et al.*, 2018). The modelling of dynamic adsorption to S950 further highlighted the effectiveness of trivalent metal removal, with the Thomas model operating capacity for Al^{3+} being an order of magnitude higher than that for the other metal species. Interestingly, Fe^{3+} had an operating capacity similar to other metal ions (Table IV), potentially suggesting that if the loading cycle was continued, Al^{3+} would be the dominant metal species remaining in the column.

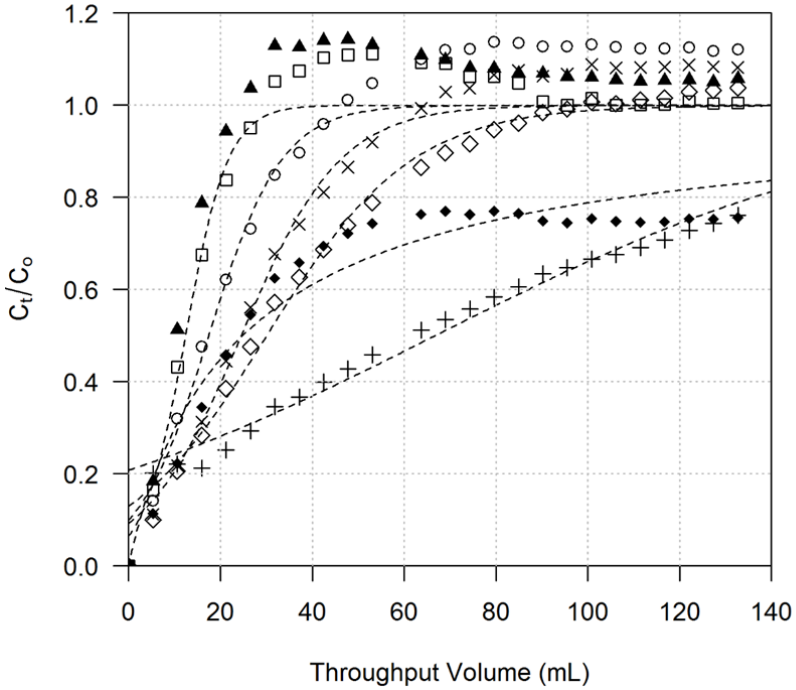

Figure 3: Breakthrough curves of metals after passing through S950 column at pH 1.43. (Al^{3+} = +, Co^{2+}= □, Cu^{2+} = ◊, Fe^{3+} = ♦, Mn^{2+} = ×, Ni^{2+} = ▲, Zn^{2+}= ○. Dotted lines represent model fitting (marked by an asterisk in Table IV).

Table IV: Selected model parameters from breakthrough analysis of S950. Asterisk (*) indicates that the model fit is displayed in Figure 3.

	Modified dose response				Bohart–Adams			Thomas		
	a	b	Q_o	R^2	K_a	*W*	R^2	K_t	Q_o	R^2
Al^{3+}	1.07	55.61	8.86	*0.959*	0.005	34.94	*0.983*	0.005	12.42	*0.983**
Co^{2+}	3.33	11.62	1.67	*0.914*	0.06	5.11	*0.936*	0.06	2.08	*0.936**
Cu^{2+}	2.21	26.62	3.53	*0.972*	0.02	11.98	*0.991*	0.02	4.66	*0.991**
Fe^{3+}	0.94	24.81	3.26	*0.905**	0.01	19.45	*0.632*	0.01	4.31	*0.632*
Mn^{2+}	2.84	22.61	3.01	*0.935*	0.03	9.53	*0.964*	0.03	3.82	*0.995**
Ni^{2+}	3.7	10.13	1.41	*0.832*	0.08	4.2	*0.853*	0.08	1.72	*0.853**
Zn^{2+}	2.94	16.09	2.26	*0.851*	0.03	7.18	*0.880*	0.03	2.86	*0.880**

Strong Acid Resin – S957

A relatively high volume of solution was passed through the S957-packed column before any metals were detected in effluent solutions (approximately 60 mL or 12 BV). During this initial period, it was assumed that all metal species were being adsorbed to the phosphonic-/sulphonic-acid functional groups. The breakthrough pattern of metals from the column can be described as three distinct groups (Figure 4). Ni^{2+}, Co^{2+}, and Zn^{2+} are first to reach complete breakthrough, with Ni^{2+} and Co^{2+} beginning to be displaced from the column after 100 mL (20 BV) throughput (Figure 4). This is due to increased loading of Cu^{2+}, Fe^{3+} and Mn^{2+}, which are also expected to eventually be displaced by Al^{3+}. Concentration ratios of Al^{3+} did not exceed 0.09 throughout the experiment, with modelling results suggesting a very high operating capacity for aluminium by S957 (Table V). Model fit R^2 values were generally reasonable (> 0.95), except for aluminium (R^2 = 0.846), which is most likely due to the low breakthrough concentration ratio.

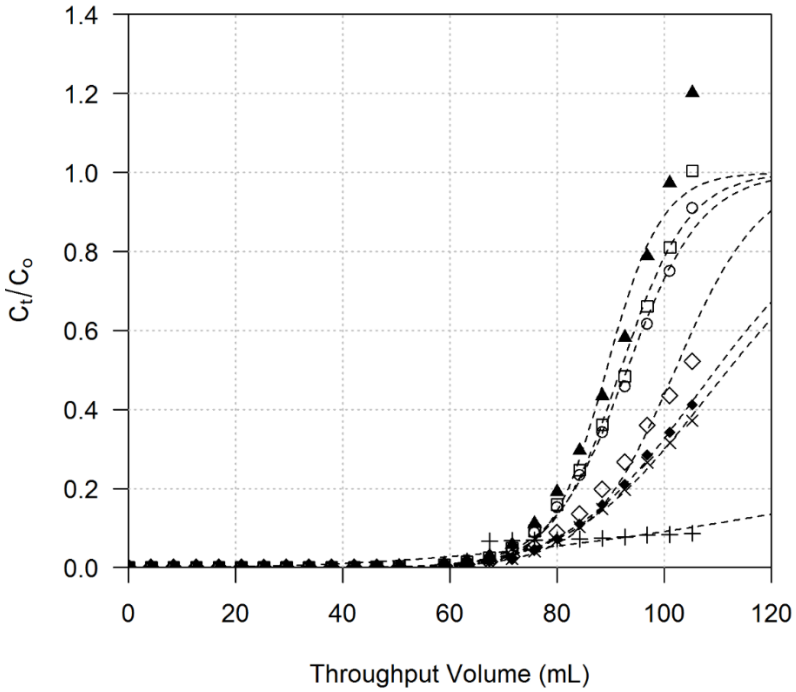

Figure 4: Breakthrough curves of metals after passing through S957 column at pH 1.43. (Al^{3+} = +, Co^{2+}= □, Cu^{2+} = ◊, Fe^{3+} = ♦, Mn^{2+} = ×, Ni^{2+} = ▲, Zn^{2+}= ○. Dotted lines represent model fitting (marked by an asterisk in Table IV).

Table V: Selected model parameters from breakthrough analysis of S957. Asterisk (*) indicates that the model fit is displayed in Figure 4.

	Modified dose response				Bohart–Adams			Thomas		
	a	*b*	Q_o	R^2	K_a	*W*	R^2	K_t	Q_o	R^2
Al^{3+}	2.46	255.08	32.40	*0.846**	0.01	32.02	*0.795*	0.01	21.60	*0.795*
Co^{2+}	14.54	91.58	10.37	*0.988*	0.04	15.41	*0.991*	0.03	10.4	*0.991**
Cu^{2+}	13.28	101.57	10.67	*0.962*	0.03	15.86	*0.964*	0.03	10.71	*0.964**
Fe^{3+}	7.92	109.56	11.67	*0.999**	0.02	17.12	*0.995*	0.02	11.56	*0.995*
Mn^{2+}	7.58	111.89	11.80	*0.997**	0.02	17.25	*0.992*	0.02	11.65	*0.992*
Ni^{2+}	17.64	88.96	9.66	*0.969*	0.05	14.35	*0.972*	0.04	9.69	*0.972**
Zn^{2+}	13.01	92.71	10.11	*0.995*	0.04	15.02	*0.997*	0.03	10.14	*0.997**

DISCUSSION

M4195 exhibited low retention of Al^{3+}, Fe^{3+} and Mn^{2+} under column operation (Figure 1). The tendency for low adsorption of these metals by M4195 at the studied pH has previously been described in the literature (Riley *et al.*, 2018), indicating similar behaviour between batch and column operation. Low Fe^{3+} retention by M4195 was reported by Canner *et al.* (2017), along with intermediate Co^{2+} uptake, which was also observed in Figure 1. The high Cu^{2+} selectivity and operating capacity strongly suggests that this resin would be suitable for treating mine tailings, as copper is commonly encountered in such wastes.

Concentration ratio of effluents from the S930 column increased rapidly, yet multiple metal species remained associated with the iminodiacetic-acid functionality throughout the experimental period (Figure 2). The presence of a tertiary nitrogen atom and two carboxyl groups causes the high Cu^{2+} extraction preference by S930 (Marhol and Cheng, 1974). The uptake of multiple species on S930 suggests that this resin could be used to remove multiple metals from tailings leachates, particularly if the Cu^{2+} was removed by M4195 prior to treatment with S930, as this would leave more capacity available for the adsorption of other divalent metals.

The chelating weak-acid resin, S950, revealed a distinct affinity towards trivalent ionic species; in this case, Al^{3+} and Fe^{3+}. The favourability towards trivalent metal extraction was also observed under static experimental conditions (Riley *et al.*, 2018), particularly under higher proton concentration. It is proposed that by placing S950 towards the back-end of a coupled-column treatment system, where proton exchange from previous columns would decrease solution pH, selective removal of trivalent metal species could be maximised. The dual-functionality resin, S957, also had a higher selectivity towards Al^{3+}, with a higher operating capacity for Al^{3+} than S950 (Table IV and V). The seemingly higher total capacity of S957, indicated by the delayed metal breakthrough in Figure 4 (also in Canner *et al.*, 2017), could be used to suggest that S957 would be more suitable for 'scrubbing' of residual metal species from the end of the treatment system. However, more research on the thermodynamics and kinetics of metal separations by S957 is required to better understand its behaviour.

CONCLUSIONS

A series of dynamic loading experiments using an artificial mine waste leach solution were carried out for several commercially available ion-exchange resins. The aim of the work was to assess the suitability of each adsorbent for its potential application in a coupled-column treatment process designed to remove problematic metals from aqueous mine wastes; either from 'naturally' occurring mine waters or from a sulphuric acid leach of mine tailings. The preliminary results presented here suggest that the contaminated solutions should first be passed through a column of M4195 to remove Cu^{2+} (and likely Ni^{2+}), followed by S950 to adsorb the trivalent metal species (Fe^{3+}, Al^{3+}), and finally S930 to remove residual divalent metals. The high capacity of S957 suggests that this could be used as a final 'scrubbing' column. The results of further experiments combining ion-exchange columns of different functionality are being awaited currently, which will help to improve and further understand the efficiency of this process prior to scale-up.

ACKNOWLEDGEMENTS

The authors would like to acknowledge the Separations and Nuclear Chemical Engineering Research (SNUCER) Group at the University of Sheffield, whose members have all assisted with this work in some capacity. Dr Will Mayes and Bob Knight from the University of Hull, in addition to the MIDAS facility, University of Sheffield, are thanked greatly for facilitating access to ICP-OES analytical equipment, without which this work would not have been possible.

NOMENCLATURE

C_t = analyte concentration at time, t; mg/L
C_o = analyte concentration at t = 0; mg/L
F_t = cumulative flow-through at time, t; L
a, b = modified dose response model constants
Q_o = maximum operational column capacity; mg/g
m = mass of resin used; g
K_a = Bohart–Adams adsorption rate constant
t = time; h
W = Bohart–Adams column adsorption capacity; mg/g
F = volumetric flow rate; L/h
K_t = Thomas model constant

REFERENCES

Albadarin, A.B., Mangwandi, C., Al-Muhtaseb, A.H., Walker, G.M., Allen, S.J. and Ahmad, M.N.M. (2012). Modelling and fixed bed column adsorption of Cr(VI) onto orthophosphoric acid-activated Lignin. *Chinese Journal of Chemical Engineering,* 20 (3), 469–477.

Amphlett, J.T.M., Sharrad, C.A. and Ogden, M.D. (2018). Extraction of uranium from non-saline and hypersaline conditions using iminodiacetic acid chelating resin Purolite S930+. *Chemical Engineering Journal*, 342, 133–141.

Armitage, P.D., Bowes, M.J. and Vincent, H.M. (2007). Long-term changes in macroinvertebrate communities of a heavy metal polluted stream: The River Nent (Cumbria, UK) after 28 years. *River Research and Applications,* 23, 997–1015.

Banks, D., Younger, P.L., Arnesen, R.-T., Iversen, E.R. and Banks, S.B. (1997). Mine-water chemistry: the good, the bad and the ugly. *Environmental Geology*, 32 (3), 157–174.

Banks, D., Athresh, A., Al-Habaibeh, A. and Burnside, N. (2017). Water from abandoned mines as a heat source: practical experiences of open- and closed-loop strategies, United Kingdom. *Sustainable Water Resources Management*, http://doi.org/10.1007/s40899-017-0094-7.

Byrne, P., Reid, I. and Wood, P.J. (2013). Changes in macroinvertebrate community structure provide evidence of neutral mine drainage impacts. *Environmental Science: Processes & Impacts*, 15, 393–404.

Canner, A.J., Pepper, S.E., Hayer, M. and Ogden, M.D. (2017). Removal of radionuclides from a HCl steel decontamination stream using chelating ion exchange resins – Initial studies. *Progress in Nuclear Energy*, 104, 271–279.

Crane, R.A., Sinnett, D.E., Cleall, P.J. and Sapsford, D.J. (2016). Physicochemical composition of wastes and co-located environmental designations at legacy mine sites in the south west of England and Wales: Implications for their resource potential. *Resources, Conservation and Recycling,* 123, 117–134.

Escudero, C., Poch, J. and Villaescusa, I. (2013). Modelling of breakthrough curves of single and binary mixtures of Cu(II), Cd(II), Ni(II) and Pb(II) sorption onto grape stalks waste. *Chemical Engineering Journal*, 217, 129–138.

Hamdaoui, O. (2009). Removal of copper(II) from aqueous phase by Purolite C100-MB cation exchange resin in fixed bed columns: Modelling. *Journal of Hazardous Materials,* 161 (2–3), 737–746.

Johnson, D.B. and Hallberg, K.B. (2003). The microbiology of acidic mine waters. *Research in Microbiology*, 154 (7), 466–473.

Kruse, N.A., DeRose, L., Korenowsky, R., Bowman, J.R., Lopez, D., Johnson K. and Rankin, E. (2013). The role of remediation, natural alkalinity sources and physical stream parameters in stream recovery. *Journal of Environmental Management*, 128, 1000–1011.

Marhol, M. and Cheng, K.L. (1974). Some chelating ion-exchange resins containing ketoiminocarboxylic acids as functional groups. *Talanta,* 21, 751–762.

Mayes, W.M., Johnson, D., Potter, H.A.B. and Jarvis, A.P. (2009). A national strategy for identification, prioritisation and management of pollution from abandoned non-coal mine sites in England and Wales. I. Methodology development and initial results. *Science of the Total Environment*, 407 (21), 5435–5447.

Mayes, W.M., Potter, H.A.B. and Jarvis, A.P. (2010). Inventory of aquatic contaminant flux arising from historical metal mining in England and Wales. *Science of the Total Environment,* 408 (17), 3576–3583.

Neymeyer, A., Williams, R.T. and Younger, P.L. (2007). Migration of polluted mine water in a public supply aquifer. *The Quarterly Journal of Engineering Geology and Hydrogeology*, 40 (1), 75–84.

Riley, A.L., Pepper, S.E., Canner, A.J., Brown, S.F. and Ogden, M.D. (2018). Metal recovery from jarosite waste – A resin screening study. *Separation Science and Technology*, 53 (1), 22–35.

Westermann, S., Dogan, T., Reker, B., Goerke-Mallet, P., Wolkersdorfer, C. and Melchers, C. (2017). Evaluation of mine water rebound processes in European Coal Mine Districts to enhance the understanding of hydraulic, hydrochemical and geomechanical processes. *Proceedings of Mine Water and Circular Economy, IMWA 2017*, Lappeenranta, Finland.

Wolkersdorfer, C. (2008). *Water Management at Abandoned Flooded Underground Mines*. Springer, Berlin, Heidelberg.

Younger, P.L., Banwart, S.A. and Hedin, R.S. (2002). *Mine Water: Hydrology, Pollution, Remediation*. Kluwer Academic, The Netherlands.